Quantum pillars: electron states and magnetic depopulation in the ideal system

1989 J. Phys.: Condens. Matter 1 7635

(http://iopscience.iop.org/0953-8984/1/41/015)

J. Phys.: Condens. Matter **1** (1989) 7635–7641. Printed in the UK

Quantum pillars: electron states and magnetic depopulation in the ideal system

M J Kelly†
Cavendish Laboratory, Madingley Road, Cambridge CB3 0HE, UK

Received 26 May 1989, in final form 10 July 1989

Abstract. In this paper, we discuss the electron states in narrow pillars (typically of sub-micrometre diameter) where the lateral confinement plays an important role in determining the transport. The present system, because of the high degree of symmetry, permits a detailed and more simple analysis of magnetic depopulation over other one-dimensional transport systems.

1. Introduction

The recent advances in the fabrication both of multilayer single crystals and of microstructures within them has permitted ever more detailed studies to be performed on the nature of electronic transport in solids. In the last two years, two types of system have been particularly studied: the use of split gates and other such gate configurations defined over the capping layer of a very high-mobility heterojunction in the GaAs/AlGaAs system (Wharam *et al* (1988), Smith *et al* (1988) and references therein), and the use of etched pillars to allow transport vertically through multilayers. The former system has the advantage that the very long distances (several micrometres) over which electrons retain their quantum phase memory between inelastic collisions can to a great extent be preserved through the electron beam microfabrication of the gate structures, and striking effects such as ballistic transport phenomena and Aharonov–Bohm oscillations have been clearly observed. Only one notable example of the use of quantum pillars for transport studies has been reported, namely the work of Reed *et al* (1988) on vertical transport through a double-barrier diode system within pillars that have external dimensions of approximately 0.25 μm (square). There they see extra structure in the current–voltage characteristics which they associate with the effects of lateral confinement on the electron states involved in the resonant tunnelling. Many other studies have been performed on the optical properties of quantum pillars where the extra technological difficulties of preparing Ohmic contacts to the top of a small pillar are not encountered. As we shall see below, this particular system has a high symmetry, and allows the entire structure to be handled analytically: indeed analytic approximations of convenience in the split-gate analyses are more appropriate here.

In this paper, some aspects of the electron states relevant to vertical transport in vertical pillars are discussed: we restrict ourselves here to a layered doping profile

† Also at GEC Hirst Research Centre, East Lane, Wembley, Middlesex HA9 7PP, UK.

0953-8984/89/417635 + 07 $02.50

in GaAs, but extensions to multilayers that include AlGaAs alloys, the effects of irregularities in the perfect structure or damage from the fabrication process, and the possible effects from lateral gating will be described in subsequent papers. Sakaki (1980) was the first to introduce the quantum wire concept, and subsequently some estimates of the transport properties were evaluated. Here we consider the regime at low temperatures where the detailed physics is likely first to be investigated.

2. The simple depletion model

Consider a vertical pillar of radius a (typically 0.1–1 μm here) etched in a multilayer of GaAs where the top and bottom contact layers are Si doped at typically $10^{24}\,m^{-3}$ while the intervening (1–2 μm thick) is doped just above the metal–insulator transition (i.e. a few $10^{22}\,m^{-3}$). We assume that a low-resistance Ohmic contact is available to the top layer to allow vertical transport studies (see figure 1). Implant isolation is an alternative fabrication technique, where those volumes outside the pillar are subject to ion implantation which damages these regions: the precise potential at the vertical implant boundaries has not been investigated, but the results here may be of relevance to this question.

In a simple depletion model, we assume that the potential for electrons is pinned at the surface such that there is a built-in voltage of $V_p \simeq 0.7$ eV. Since the whole question of the surface electronic potential of semiconductor microstructures is of direct device relevance, e.g. in microwave MESFET and HEMTs, we should hope to invert some of the results here to infer the value and variation of the surface pinning of the potential. The depletion depth $\sqrt{(2\varepsilon_s V_p/eN_d)}$ for an electron of charge e and donor density N_d is $\simeq$30 nm for $10^{24}\,m^{-3}$ doping while it is $\simeq$300 nm for $10^{22}\,m^{-3}$ doping density. On this scale, in a circular pillar of radius $\simeq$0.1 μm, the resistance of any structure will be dominated by the thin, nearly depleted, region of the low-doped layer.

If we assume that the free carriers collect in the centre of the pillar (see the justification below) then the solution to the Poisson equation for the depletion profile in the circular geometry is straightforward, namely

$$\varphi(r) = V_p + (N_d e/4\varepsilon_s)(r^2 - a^2)$$

which also survives with the addition of a term Fz if an electric field F is applied along the wire. This result is used in the analysis of their data by Reed *et al* (1988). We shall return subsequently to the problem of a varying doping density, i.e. $N_d(z)$, although some cases, e.g. a doping superlattice, admit analytic solutions.

3. The electron states

The parabolic form of the radial potential is precise within the depletion approximation, which makes the solution for the electron wavefunctions straightforward. Furthermore the 'stiffness' of the confining potential depends only on the measurable N_d, and, as we shall see below, it can be modified systematically with an applied magnetic field. The analytic simplicity that features here is only an approximation, and a convenience, in the split-gate heterojunction work, and in that system only for the lateral rather than depth confinement. The one-electron Schrödinger equation

$$-(\hbar^2/2m^*)\nabla^2\psi + (N_d e^2 r^2/4\varepsilon_s)\psi = E\psi$$

defined with respect to the potential at the centre of the pillar, has two-dimensional

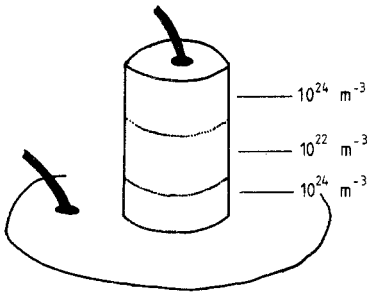

Figure 1. A schematic diagram of the structure we examine in this paper.

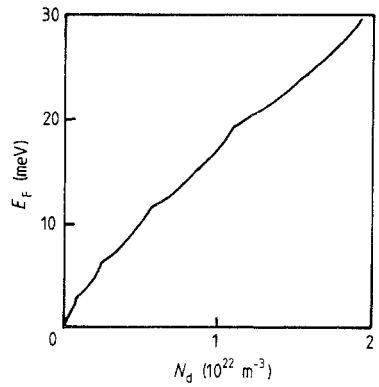

Figure 2. The Fermi energy as a function of carrier concentration: the break in slope occurs as each new sub-band is occupied.

oscillator wavefunctions in the radial direction so the wavefunctions are (Landau and Lifshitz 1977, Wallace 1984)

$$\psi = D_{nm}(r/a^*)^{|m|} \exp[-(r/a^*)^2/2]L_n^{(m)}[(r/a^*)^2] \exp(im\theta) \exp(ik_z z)$$

(where m is an integer and n a non-negative integer) with one-dimensional sub-bands for the vertical motion characterised by an effective mass m^*, while the eigenenergies and the mean diameters of the wavefunctions are given by

$$E(n, m, k_z) = \hbar\omega(2n + |m| + 1) + \hbar^2 k_z^2/2m^*$$

$$\omega = \sqrt{(N_d e^2/2\varepsilon_s m^*)} \qquad \sqrt{\langle a^{*2}\rangle} = \sqrt{(E_{0,0,0}/m^*\omega^2)}$$

and have typical values of 30 meV and 11 nm for 10^{24} m^{-3} doping and 3 meV and 30 nm for 10^{22} m^{-3} doping, justifying the initial assumption for calculating the electron distribution. The Fermi energy as a function of electron density is also simple to evaluate, since the number of electrons per unit length is given by integrating the filled bands to E_F

$$N_d \pi a^2 = \sum_{j=1} \int_{j\hbar\omega} (1/\pi)\sqrt{(2m^*/\hbar^2)}j/\sqrt{(E - j\hbar\omega)}\, dE.$$

Note that, since $\hbar\omega$ is proportional to $\sqrt{N_d}$, and if we anticipate the magnetic field results and use $E_0 = 2\hbar\omega$ as a unit of energy, we can rewrite this equation as

$$0.0324a^2 N_d^{0.75} = \sum_j j\sqrt{(f - j/2)} \tag{1}$$

where f is the Fermi energy expressed in units of E_0, and the numerical prefactor includes all the fundamental constants, together with a relative permittivity of 12 and an effective mass of $0.67m_e$ peculiar to GaAs. The prefactor j relates to the degeneracy of sub-band energies for different n and m quantum numbers. The occupation of the sub-bands as N_d increases for a pillar of 0.1 μm radius is shown in figure 2, and is qualitatively similar to that encountered in other quasi-1D systems. A self-consistent solution of the Schrödinger and Poisson equations, incorporating the electronic potential, will, for

many occupied sub-bands, flatten out the potential well in the manner of Laux *et al* (1988), as described in § 5 below.

4. Magneto-electron states

With the presence of a magnetic field along the axis of the wire, the Schrödinger equation becomes

$$-(\hbar^2/2m^*)\nabla^2\psi - (e/2m^*)(\boldsymbol{A}\cdot\boldsymbol{p} + \boldsymbol{p}\cdot\boldsymbol{A})\psi + (e^2A^2/2m^*)\psi + kr^2/2\psi = E\psi$$

where $k = (e^2N_d/2\varepsilon_s)$. With the gauge in which $\boldsymbol{A} = 0.5\boldsymbol{B}\times\boldsymbol{r}$, the solutions are now

$$E = \hbar\omega_H\sqrt{(1 + 4k/m^*\omega_H^2)}(n + |m|/2 + \tfrac{1}{2}) + m\hbar\omega_H/2 + (\hbar^2k_z^2)/2m^*$$

(here $\omega_H = eB/m^*$ and n (a non-negative integer) and m (an integer) are the radial and angular quantum numbers of an axially symmetric solution), and the wavefunction is given by

$$\psi(r) = D_{nm}(r/a_H)^{|m|}\exp(-r^2/2a_H^2)F(-n, |m| + 1, r^2/2a_H^2)\exp(im\theta)\exp(ik_z z)$$

$$a_H = (\hbar/2m^*\omega_H)^{0.5}(1 + 4k/m^*\omega_H^2)^{-0.25}$$

(see Landau and Lifshitz (1977), p 458, for details, although here one must make a further, and simple, rescaling to account for the additional confinement from the magnetic vector potential). Note here that the longitudinal mass is unaffected. To proceed, we define $\alpha = m^*\omega_H^2/4k = e^2B^2/4km^*$ as a measure of the ratio of the magnetic radial confinement from the $e^2A^2/2m^*$ term above to the dopant confinement (k); we see that the two effects act to provide the overall radial confinement, although the magnetic field contributes an extra axial term. The equivalent to equation (1) is now

$$0.0324a^2N_d^{0.75} = \sum_{nm}\sqrt{\{f - [\sqrt{(1+\alpha)}(n + |m|/2 + \tfrac{1}{2}) + \sqrt{\alpha}m/2]\}} \qquad (2)$$

where the reduced Fermi energy f is again measured in terms of the same E_0 as above, and the summation is over all occupied sub-bands. Note that in the limit of $\alpha \simeq B^2 \to 0$, the previous equation (1) is recovered, including all the degeneracy factors. The shifts of the $\pm m$ energy levels are different, and the overall pattern of energy levels is complex, especially in the region where $\alpha \simeq 1$, there being quite different limits when $\alpha \ll 1$ and $\alpha \gg 1$. The plot of E_F versus B for fixed N_d, as shown in figure 3, is a result of the depopulation of the energy levels.

When a magnetic field is applied at right angles to the wire (say in the x direction) then the solution for the Schrödinger equation

$$(\hbar^2/2m^*)\nabla^2\psi - (i\hbar e/m^*)By\delta\psi/\delta z + (e^2B^2/2m^*)y^2\psi + 0.5k(x^2 + y^2)\psi = E\psi$$

is more complex, involving a shift of the y-coordinate frame to a centre at $y_0 = -(\hbar eBk_z/m^*)/(k + e^2B^2/m^*)$ to give two independent harmonic oscillator solutions (by separation of variables), but with different characteristic energies. At the same time,

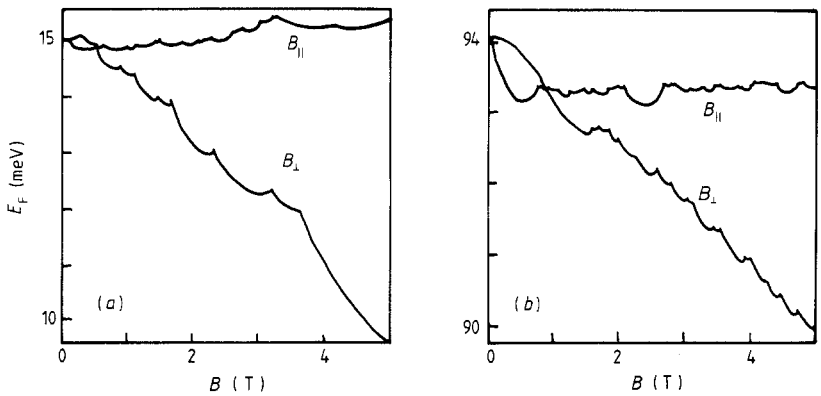

Figure 3. The Fermi energy as a function of magnetic field both parallel and perpendicular to the axis of the wires for bulk material doping densities of (*a*) $10^{22}m^{-3}$ and (*b*) $10^{23}m^{-3}$, showing the effects of depopulation of the various magneto-electron 1D sub-bands.

this shift also results in an increase in the k_z effective mass, and the solution now (see Landau and Lifshitz 1977, Wallace 1984) is

$$E = n_1\hbar\sqrt{(k/m^*)} + n_2\hbar\sqrt{[k(1+4\alpha)/m^*]} + (\hbar^2k_z^2/2m^*)/(1+4\alpha)$$

where all terms have their previously defined meaning, and both n_1 and n_2 are non-negative integers. The equivalent to equations (1) and (2) is

$$0.0324a^2N_d^{0.75} = \sum_{n_1,n_2}(1+4\alpha)\sqrt{\{f - [n_1 + (1+4\alpha)n_2 + 1)/2\}} \qquad (3)$$

which has the same limit as $\alpha \to 0$, but the n_1, n_2 and n, m are different representations of the 2D harmonic oscillator solutions. Here we note an increase in the effective mass in the z direction, which affects the density of states of the 1D sub-bands, and which should also manifest itself in transport as a positive magnetoresistance, at least in the Drude transport regime. The steep decrease in E_f when the magnetic field is perpendicular to the pillar is entirely due to this increase in longitudinal effective mass. The magnetic depopulation now proceeds in a different manner than in the case where the magnetic field is parallel to the wire (see figure 3).

Given the typical systems that have been evaluated in figure 3, magnetotransport could now be used to calibrate the doping density in the thin layer, and extra depletion corrections that arise from non-uniform doping depth profiles. If deviations from this simple picture are observed in practice, they might arise from one of several complicating factors to which we turn below. Note that proton isolation is an alternative method for producing the defined vertical pillar as mentioned above, and these techniques may prove the nature of the pinning of the potential at the edge of the implant region.

5. The self-consistent Poisson–Schrödinger equation

The self-consistent solution of the Poisson–Schrödinger equation involves incorporating the potential of the electrons into the Schrödinger equation. In the case of the split-gate 1D systems (Laux *et al* 1988), the self-consistency flattens out the potential in the bottom of the well (i.e. the centre of our pillar), and reduces the inter-level energy spacings.

This is a major task, even in the present simple system, but we can make a crude estimate of its importance by integrating the Poisson equation for the electrons in the lowest sub-band, and calculating the potential energy contribution (in a mean-field sense). The solution of

$$(1/r)(\delta/\delta r)(r\,\delta V/\delta r) = \rho(r)/\varepsilon_s = e^2 n|\psi(r)|^2/\varepsilon_s$$

is

$$V(r) = -(e^2 n/4\pi\varepsilon_s)[E_1(r^2/a^{*2}) + \ln(r^2/a^{*2}) + \gamma]$$
$$= (e^2 n/4\pi\varepsilon_s)[(r/a^*)^2 - 0.25(r/a^*)^4 + 0.06(r/a^*)^6 \ldots]$$

where E_1 is the exponential integral, $\gamma = 0.577\ldots$, and $n = \pi a^2 N_d$ is the line density of electrons. The contribution to the potential energy is then

$$\int eV(r)\rho(r)\,r\,\mathrm{d}r = -(e^2 n/4\pi\varepsilon_s)\ln 2.$$

This represents a significant correction, which implies a widening of the potential wells, a reduction in the inter-level separation, and a consequent increase in the relative importance of the magnetic fields. Indeed, if one adds this self-consistent potential of the electrons to the depletion potential, the r^2 term in the potential exactly cancels, at least for $r < a^*$. In the range of parameters typical of the systems considered, the change from an r^2 to a $0.25r^4$ potential results in separation of the energy levels for radial quantum numbers being reduced to a third of the values in §§ 3 and 4 above, and of course the potential near the centre of the pillar is flatter, just as in Laux *et al* (1988). Of course with electrons in upper energy sub-bands, the self-consistent potential will not be as simple as just described. It may be that magnetic depopulation studies might be used to probe the self-consistent potentials appropriate to the present system. Further work on this aspect is in progress.

6. Screening

Much of the pertinent work on the dielectric response of a one-dimensional electron gas has been performed by Das Sarma and Lai (1985) for narrow heterojunction channels appropriate to the split-gate system. In our case further analytic progress is possible, with the ground-state Coulomb interaction matrix element being given by

$$V(q) = (2e/\varepsilon_s)\left(0.5\exp(-q^2/2)\int_{q^2/2}^{\infty}\exp(-t)/t\,\mathrm{d}t\right)$$

the integral being tabulated, and which gives (for $qa < 1$) results very close to those of the purely 1D calculation of Das Sarma and Lai, except that it falls off more rapidly for larger q. The more important aspect is that, with many sub-bands occupied, the other Coulomb matrix elements are much smaller (e.g. by a factor of approximately 16 even within the first excited sub-band). The plasmon frequency derived by Das Sarma and Lai is of the form

$$\omega_p \sim \omega_0(qa)\sqrt{K_0(qa)}$$

where K_0 is the modified Bessel function of the second kind (which can be related to the exponential integral form used in the expression of $V(q)$ above). For practical systems

the $\omega_0 = \sqrt{(2ne^2/\varepsilon_s m^* a^2)}$ can be as large as 60 meV, but in the case of many occupied sub-bands, a somewhat smaller effective line charge density n ($=\pi a^2 N_d$) is appropriate.

7. Conclusion

The quantum pillar offers a simple system for the investigation of quasi-one-dimensional electron states and conduction. It has advantages of symmetry over many other quasi-1D systems. The large lattice mass compared with those of the conducting polymers such as TTF-TCNQ means that the electron–phonon instabilities are unlikely to be seen. The results of figure 3 can be modified to describe the recent experimental results (Hansen *et al* 1989) on depopulation of quantum dots where electrons are confined laterally in the same manner as here, but in the vertical direction a heterojunction HEMT-type potential confines motion.

Acknowledgment

The work at Cambridge was supported in part by a Royal Society/SERC Industrial Fellowship.

References

Das Sarma S and Lai W 1985 *Phys. Rev.* B **32** 1401–4

Hansen W, Smith T P III, Lee K Y, Brum J A, Knoedler C M, Hong J M and Kern D P 1989 *Phys. Rev. Lett.* **62** 2168–71

Landau L D and Lifshitz E M 1977 *Quantum Mechanics* (Oxford: Pergamon)

Laux S E, Frank D J and Stern F 1988 *Surf. Sci.* **196** 101–6

Reed M A, Randall J N, Aggarwal R J, Matyi R J, Moore T M and Wetsel A E 1988 *Phys. Rev. Lett.* **60** 535–8

Sakaki H 1980 *Japan. J. Appl. Phys.* **19** L737–8

Smith C G, Pepper M, Ahmed H, Frost J E F, Hasko D G, Peacock D C, Ritchie D A and Jones G A C 1988 *J. Phys. C: Solid State Phys.* **21** L893–8

Wallace P R 1984 *Mathematical Analysis of Physical Problems* (New York: Dover)

Wharam D A, Thornton T J, Newbury R, Pepper M, Ahmed H, Frost J E F, Hasko D G, Peacock D C, Ritchie D A and Jones G A C 1988 *J. Phys. C: Solid State Phys.* **21** L209–13